Invariance of Structure in an Aging Colloidal Glass

Gianguido C. Cianci*, Rachel E. Courtland* and Eric R. Weeks*

*Department of Physics, Emory University, Atlanta, GA 30322, U.S.A.

Abstract. We study concentrated colloidal suspensions, a model system which has a glass transition. The non-equilibrium nature of the glassy state is most clearly highlighted by aging – the dependence of the system's properties on the time elapsed since vitrification. Fast laser scanning confocal microscopy allows us to image a colloidal glass and track the particles in three dimensions. We analyze the static structure in terms of tetrahedral packing. We find that while the aging of the suspension clearly affects its dynamics, none of the geometrical quantities associated with tetrahedra change with age.

INTRODUCTION

If a liquid is rapidly cooled faster than it can crystallize, it can form an amorphous solid also known as a glass. This occurs below a temperature known as the glass transition temperature, T_g. As T_g is approached from above, the viscosity of the liquid increases by many orders of magnitude over a small range in temperature. However, a diverging structural length scale that would also grow by orders of magnitude and thus explain this thickening has not been identified [1–5].

A related phenomenon is that of aging [6, 7], the observation that a glassy sample is not in equilibrium and thus its properties depend on the age of the sample. Were the system able to equilibrate at or below T_g it would assume the lowest energy configuration: a crystal. However upon a temperature quench to $T < T_g$ the system's dynamics are severely slowed and its structure is frozen in an amorphous configuration. Slight thermal motions do survive this temperature quench and slowly allow the system to change configurations albeit in a non-ergodic fashion. The time scale for rearrangements grows with the age of the sample; the older the sample, the longer the time needed for a further change. Similarly to the problem of the glass transition, a changing time scale for aging dynamics is suggestive of an underlying changing structural length scale. One conjecture is that as the glass ages it optimizes its packing. Specifically the length scale over which some "optimal packing" is achieved might grow during aging, thus slowing the dynamics of the sample, which in turn would slow the aging process itself.

Suspensions of colloids have been studied as a model glass-forming system with great success. Colloidal suspensions consist of solid particles in a liquid, and exhibit a glass transition as their concentration is increased. In such systems, the control parameter is not temperature but packing fraction, ϕ, and a glass is obtained once ϕ increases above $\phi_g \approx 0.58$ [8–11]. Previous work with colloids [12, 13] has shed some light on the aging process showing, for example, that aging is both spatially and temporally heterogeneous. However a detailed understanding of the microscopic mechanisms involved is still lacking.

In this work we analyze aging in a colloidal glass from a geometrical point of view. In particular we focus on the idea of geometrical frustration [14, 15]. In hard sphere systems the free energy is exclusively determined by entropy and, in order to minimize the former at a given temperature, the system has no choice but to maximize the latter. This is evident already at a packing fraction of $\phi_{\text{crystallization}} \approx .494$ where the system crystallizes, despite the lack of inter-particle interactions, sacrificing some configurational entropy to gain vibrational entropy instead [16]. This is achieved by re-distributing the available space homogeneously so that all particles have more local free volume and thus room to move about their average lattice position.

The most efficient packing of four spheres in three dimensions is to pack them into a regular tetrahedron. The effective volume fraction of four such spheres is $\phi_{\text{tetrahedron}} \approx 0.78$. However regular tetrahedra don't tile 3-D space, and thus the most efficient space filling configuration is a hexagonally closed packed crystal with $\phi_{\text{hcp}} \approx 0.74$. So while tetrahedral packing could locally maximize vibrational entropy, the constraint that the sample fill space induces crystallization. This *frustration* between local and global packing optimization has been invoked as a possible cause for the glass transition in simple liquids [14, 15].

We use fast laser scanning confocal microscopy to observe micron-sized particles in a colloidal glass in three

CP832, *Flow Dynamics, The Second International Conference on Flow Dynamics*
edited by M. Tokuyama and S. Maruyama

dimensions. Specifically we study the static structure of the glass in terms of tetrahedral packing and analyze the evolution of some geometrical properties as the sample ages. While the dynamics change dramatically over the course of our experiment, we find no change in the structural properties, as characterized by tetrahedra arrangements.

EXPERIMENTAL DETAILS

We use poly(methyl methacrylate) (PMMA) particles of diameter $d = 2.36\mu m$ and polydispersity $\sim 5\%$. The particles are sterically stabilized by a thin layer of poly-12-hydroxystearic acid, dyed with rhodamine 6G and suspended in a mixture of cyclohexylbromide and decalin (85:15 by weight) that closely matches both the density and index of refraction of the particles. This is done to minimize sedimentation effects and to improve imaging. The solvent's viscosity at 295 K is $\eta = 2.25$ mPa·s which sets the time required to diffuse a distance d in the *dilute* limit to $\frac{d^2}{6D} = \tau_{\rm diff} = 11s$ where $D = \frac{k_B T}{3\pi\eta d}$.

We use a confocal microscope to acquire three-dimensional images of a viewing volume of 62 $\mu m \times$ 58 $\mu m \times$ 10 μm at a rate of 1 frame every 26 s. Note that the sample is glassy – at these densities the colloids move very slowly. The particles can be tracked even though the frame rate is comparable to $\tau_{\rm diff}$. The viewing volume typically contains ~ 2500 particles. We focus at least 60 μm away from the cover slip of the sample chamber to avoid wall effects [19, 20]. We identify particles with a horizontal accuracy of 0.03 μm and a vertical accuracy of 0.05 μm, and track them in three dimensions over the course of the experiment [17, 18].

The control parameter for colloidal phase behavior is the sample volume fraction ϕ. While the rhodamine imparts a slight charge upon the particles, their phase behavior, $\phi_{\rm freeze} = 0.38$ and $\phi_{\rm melt} = 0.42$, is similar to that of hard spheres ($\phi_{\rm freeze} = 0.494$ and $\phi_{\rm melt} = 0.545$). We observe a glass transition at $\phi_g \approx 0.58$, in agreement with what is seen for hard spheres. We examine samples with volume fractions in the range $\phi \approx 0.58 - 0.62$ and find qualitatively identical results. These samples form small crystals which nucleate at the cover slip, but do not form crystals within the bulk of the sample even after several weeks. Here we report results based on a sample at $\phi \approx 0.62$.

The sample is initialized by vigorous stirring. The subsequent particle dynamics are reproducible after this stirring, and depend only on the waiting time t_w since the start of the aging process. Within a minute of ending the stirring, transient flows within the sample greatly diminish, and the particles move slowly enough to be identified and tracked. This defines our initial time $t_w = 0$, or age zero, for the sample. The results below are not sensitive to variations of this choice. During the experiments, no crystallization is observed within the viewing volume. Note that in many aging studies, the initial sample is prepared by a temperature quench (corresponding to a rapid increase of the volume fraction in our experiments). The initial conditions in our experiments correspond to a shear-melted sample; the volume fraction remains constant.

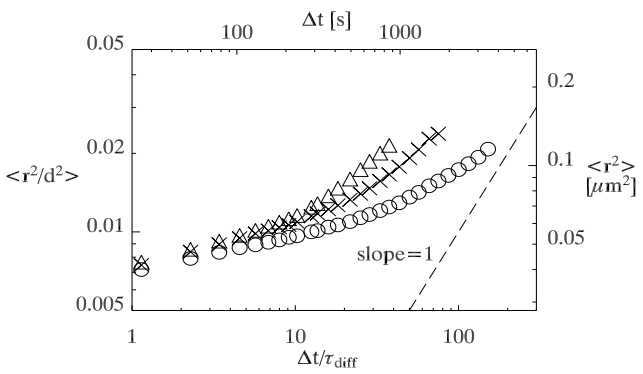

FIGURE 1. Aging mean squared displacement for a colloidal glass at $\phi \approx 0.62$. The three curves represent three different ages of the sample. $\triangle : t_w = 0\tau_{\rm diff}$, $\times : t_w = 100\tau_{\rm diff}$ and $\bigcirc : t_w = 300\tau_{\rm diff}$. The dashed line has a slope of 1 and represents diffusive behavior, not seen in this glassy sample.

Henceforth all numerical values will be expressed in terms of particle diameter d and characteristic diffusion time $\tau_{\rm diff}$.

RESULTS

In order to determine whether our sample is aging we take a long ($\sim 700\tau_{\rm diff}$) data set and split it in three time windows as follows: $[0 - 100\tau_{\rm diff}]$, $[100 - 300\tau_{\rm diff}]$ and $[300 - 700\tau_{\rm diff}]$. Since the sample is not disturbed during observation this is equivalent to running three experiments with $t_w = 0$, 100, and $300\tau_{\rm diff}$ from the sample initialization. We then measure the mean squared displacement for the three data sets averaged over all particles and over all initial times within a given window. As can be seen in Fig. 1 the data clearly show a slowing down of the dynamics. For example, as the sample ages (t_w goes from 0 to $300\tau_{\rm diff}$) the time particles take to diffuse, say, a distance of $0.02d^2$ goes from approximately $\Delta t \approx 60\tau_{\rm diff}$ to $\Delta t \approx 180\tau_{\rm diff}$.

While the dynamics are clearly changing with the age of the sample, we wish to consider the static structure as well. We start by calculating the pair correlation function $g(r)$. The resulting curve is plotted in Fig. 2, which has

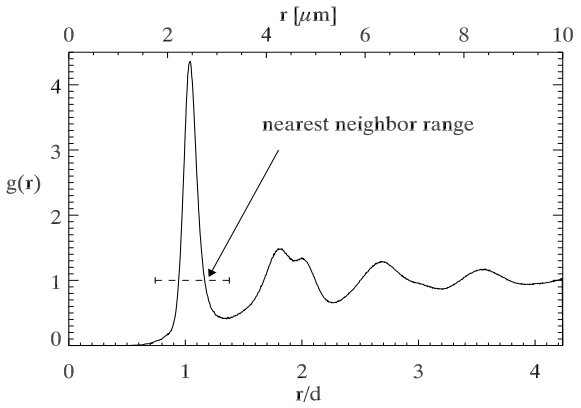

FIGURE 2. Pair correlation function for a sample with $\phi \approx 0.62$. The dashed segment indicates the range of interparticle distances used as a definition of nearest neighbor.

been calculated from data averaged over all ages of the sample; no change in $g(r)$ is seen as the sample ages. The first peak of $g(r)$ is at $r = 1.04d$, slightly displaced from the ideal hard-sphere position of $r = d$. This is mainly due to a slight charge induced by the dyeing process, and may also be due to some uncertainty in the exact value of the average particle size d which we estimate to be 2%. Another effect of this soft potential is that $g(r)$ for $r < d$ does not fall to zero as sharply as it would for perfect hard spheres. Figure 2 also shows the characteristic double peak around $r = 2d$ seen in many glassy systems.

To further characterize the geometry of the colloidal glass we identify tetrahedra formed by the particles as follows. Two colloids are labeled as nearest neighbors if their distance is within the first peak of $g(r)$, namely, if $0.74d > r > 1.38d$ as shown in Fig. 2. The upper bound corresponds to the first minimum of $g(r)$ while the lower bound is set to eliminate some nearest neighbor pairs that are excessively close to each other as a result of occasional errors in particle tracking. The results presented here are insensitive to variations in the limits for r and to the use of Delaunay triangulation as an alternative nearest neighbor finding method.

A tetrahedron is then defined as a quadruplet of mutually nearest neighbor colloids. The six inter-particle distances, or "bond" lengths, b_i with $i = 0...5$ are measured. We then assign to each tetrahedron a "looseness" as measured by the average bond length b and an "irregularity" as measured by the standard deviation of the six bond lengths σ_b and defined by $\sigma_b^2 = \sum_{i=0}^{5}(b - b_i)^2$. Note that the looseness has the same limits as the nearest neighbor distance ($b \in [0.74d, 1.38d]$) while the irregularity is bound by zero (for an ideal tetrahedron) and by the maximum of the standard deviation of six numbers drawn from the interval $[0.74, 1.38]$, namely $\sigma_b \in [0, 0.35d]$.

FIGURE 3. Computer generated picture of a very regular tetrahedron ($\sigma_b = 0.02d$, left) and a very irregular one ($\sigma_b = 0.22d$, right). The spheres are drawn to scale ($d = 2.36\mu m$).

Figure 3 shows a computer rendered image of a very regular and a very irregular tetrahedron with $\sigma_b = 0.02d$ and $\sigma_b = 0.22d$ respectively. Clearly our definition of what constitutes a tetrahedron combined with the range we set for nearest neighbor distances allows for fairly irregular, quasi planar tetrahedra; though setting $r_{max} = 1.38d < \sqrt{2}d$ avoids the possibility of a perfectly planar configuration.

Since aging is the evolution of the system's properties over times much longer than τ_{diff} we analyze these two static quantities, b and σ_b, as the sample ages. If aging is a result of thermal fluctuations slowly trying to resolve the frustration we referred to above, then one might expect the geometrical characteristics of the tetrahedra forming the sample to evolve with time. We therefore tracked the values of $\langle b \rangle$ and $\langle \sigma_b \rangle$ averaged over all tetrahedra in each frame as the sample ages, and show this in Fig. 4. These two average quantities remain essentially constant over the duration of the experiment. $\langle b \rangle$ varies by less than 0.5%, reflecting the fact that the packing fraction ϕ remains constant. One could envisage that a change in the value of $\langle \sigma_b \rangle$ would allow the sample to find a configuration with lower energy. For example, a "better packed" configuration might have fewer irregular tetrahedra, as is the case for a crystal. Such a configuration might allow each particle to have more local room to move, thus increasing its vibrational entropy. This however is not the case, as is seen in Fig. 4, which shows that $\langle \sigma_b \rangle$ decreases by less than 0.5% throughout the experiment. While a decrease is consistent with our argument, this decrease is not reproducible in other samples, and in fact we find in all cases that $\langle \sigma_b \rangle$ varies by at most 1% with no preference for increasing, decreasing, or merely fluctuating.

As neither of these average static quantities evolve as the sample ages, we consider a more complete picture by calculating the probability distribution functions $P(b/d)$ and $P(\sigma_b/d)$. For each value of the t_w the distributions were calculated by averaging over all tetrahedra and all times in each time window.

The distribution of average bond lengths $P(b/d)$ is shown in Fig. 5 and is peaked at $b/d \approx \langle b/d \rangle = 1.09$. $P(b/d)$ is approximately a Gaussian with a width of 0.04,

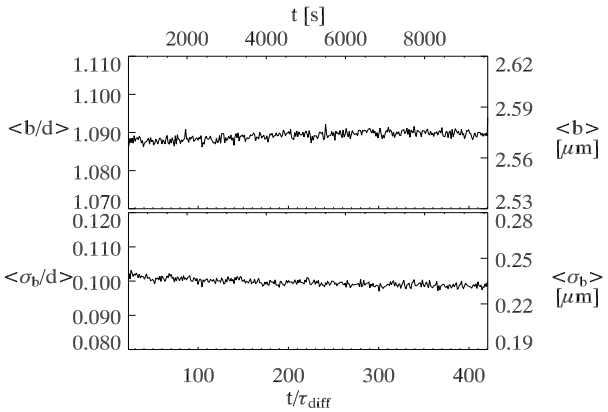

FIGURE 4. Plot of the average tetrahedral "loosness" $\langle b \rangle$ (top) and average tetrahedral irregularity $\langle \sigma_b \rangle$ (bottom) versus time. The average is taken over all tetrahedra at each time.

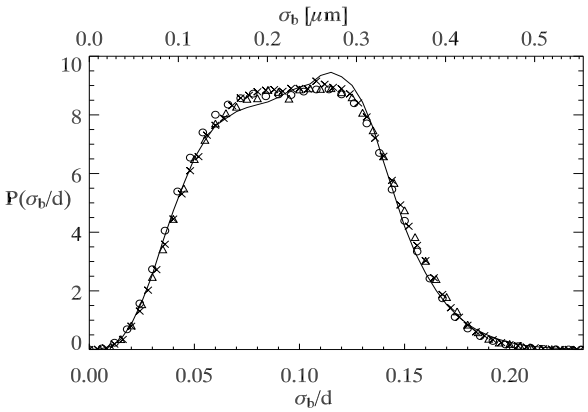

FIGURE 6. The distribution function $P(\sigma_b/d)$ for tetrahedral "irregularity" for three ages: $\triangle : t_w = 0$, $\times : t_w = 100\tau_{diff}$, and $\bigcirc : t_w = 300\tau_{diff}$. The solid line is a reference curve computed by considering random bonds based on $g(r)$, without the constraint that such bonds form a tetrahedron.

although the distribution is slightly asymmetric with a bias toward larger values of b. Thus compact tetrahedra ($b/d < 1.05$) are less prevalent, along with loose tetrahedra ($b/d > 1.13$). More significantly, the distribution $P(b/d)$ is unchanged during aging, as is seen by the excellent agreement between the distributions plotted with the different symbols. Thus, while both compact and loose tetrahedra are less likely, their relative prevalence remains unchanged as the sample ages. This seems somewhat surprising, as entropy might favor a more standardized tetrahedron size. Compact tetrahedra have less room for their particles to move; the opposite is true for loose tetrahedra. The system could maximize its overall vibrational entropy by sharing free volume more evenly. However, this is not reflected in the data, and may indicate that random packing requires both compact and loose tetrahedra in order to tile space. Thus, the age of the sample is not detected by $P(b/d)$.

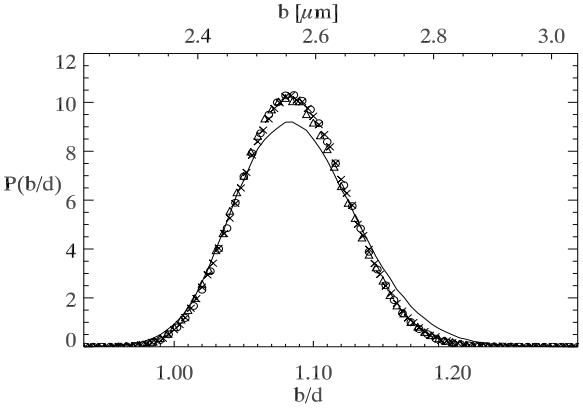

FIGURE 5. The distribution function $P(b/d)$ for tetrahedral bond lengths ("looseness") for three ages. $\triangle : t_w = 0$, $\times : t_w = 100\tau_{diff}$, and $\bigcirc : t_w = 300\tau_{diff}$. The solid line is a reference curve computed by considering random bonds based on $g(r)$, without the constraint that such bonds form a tetrahedron.

Now consider the distribution of tetrahedral irregularities $P(\sigma_b/d)$ plotted in Fig. 6. The most striking feature is a broad maximum around $\sigma_b/b \approx 0.1$. This is congruent with the amorphous quality of a glassy packing where, unlike in a crystal, one might expect to find a great variety of tetrahedra, from quite regular to quite irregular ones. However, it is also interesting to note that the probability of finding a tetrahedron with an irregularity greater than 0.2 is effectively zero while the theoretical maximum for σ_b/d is 0.35. Also, while not very regular, the shape of $P(\sigma_b/d)$ is qualitatively reproducible with other samples above ϕ_g.

The striking agreement in the tetrahedral properties between different ages of the sample suggests that there may be a simple underlying explanation for these distributions. One hypothesis is that the shape of these distributions is dictated by the statistics of choosing six bond lengths b_i at random from the overall distribution $P(b_i)$ in an amorphous configuration. $P(b_i)$ is closely related to $g(r)$ by $P(r) = r^2 g(r)$. By randomly picking many sets of six b_i, without the constraint that they form a tetrahedron, we can compute reference distributions $P'(b/d)$ and $P'(\sigma_b/d)$. These are shown as solid lines in Figs. 5 and 6. While these are similar to the experimental data, deviations are clearly seen. In Fig. 5, the solid curve shows a slight bias toward larger values of b/d as compared with the experimental data. In Fig. 6, the peak of the distributions differs noticeably between the experimental values and the reference curve. While these differences are not extreme, they are outside of the uncertainty of the data, and thus indicate that tetrahedral

properties do possess additional information beyond just nearest neighbor bond lengths [which in turn are related to $g(r)$].

CONCLUSION

We have examined an aging colloidal glass by looking at static structural characteristics of tetrahedral packing. We find that there is no correlation between the age of a glass and its static structure as evaluated by these quantities. Nevertheless, our sample's "awareness" of its age must be encoded in the particle positions, and thus in some feature of the packing of the particles. We have checked other geometrical quantities based on tetrahedral structure, such as volume or surface area, and none of these show aging either. Tetrahedral properties appear not to reflect the age and thus a static measure of a sample's age remains elusive.

ACKNOWLEDGMENTS

We thank Carrie Nugent and Ted Brzinski for useful discussions. This work was supported by NASA microgravity fluid physics grant NAG3-2728. For correspondence contact ERW: weeks@physics.emory.edu.

REFERENCES

1. C. A. Angell, *Science* **267**, 1924-1935 (1995).
2. F. H. Stillinger, *Science* **267**, 1935-1939 (1995).
3. M. D. Ediger, C. A. Angell, S. R. Nagel, *J. Phys. Chem.* **100**, 13200-13212 (1996).
4. C. A. Angell, *J. Phys. Cond. Mat.* **12**, 6463-6475 (2000).
5. N. Menon and S. R. Nagel, *Phys. Rev. Lett.* **73**, 963-966 (1994).
6. W. Kob, J. L. Barrat, F. Sciortino, P. Tartaglia, *J. Phys. Cond. Mat.* **12**, 6385-6394 (2000).
7. W. van Megen, T. C. Mortensen, S. R. Williams, and J. Müller, *Phys. Rev. E* **58**, 6073-6085 (1998); L. Cipelletti, S. Manley, R. C. Ball, and D. A. Weitz, *Phys. Rev. Lett.* **84**, 2275-2278 (2000).
8. P. N. Pusey and W. van Megen, *Nature* **320**, 340-342 (1986).
9. A. van Blaaderen and P. Wiltzius, *Science* **270**, 1177-1179 (1995).
10. I. Snook, W. van Megen and P. N. Pusey, *Phys. Rev. A* **43**, 6900-6907 (1991).
11. E. R. Weeks, J. C. Crocker, A. C. Levitt, A. Schofield, and D. A. Weitz, *Science* **287**, 627-631 (2000).
12. R. E. Courtland and E. R. Weeks, *J. Phys.: Condens. Matter* **15**, S359-S365 (2003).
13. L. Cipelletti, H. Bissig, V. Trappe, P. Ballesta and S. Mazoyer, *J. Phys.: Condens. Matter* **15**, S257-S262 (2003).
14. D. R. Nelson and M. Widom, *Nucl. Phys. B* **240**, 113-139 (1984).
15. D. R. Nelson, *Defects and Geometry in Condensed Matter Physics*, Cambridge: Cambridge University Press (2002).
16. W. G. Hoover and F. H. Ree, *J. Chem. Phys* **49**, 3609-3617 (1968).
17. A. D. Dinsmore, E. R. Weeks, V. Prasad, A. C. Levitt, and D. A. Weitz, *App. Optics.* **40**, 4152-4159 (2001).
18. J. C. Crocker and D. G. Grier, *J. Colloid Interface Sci.* **179**, 298-310 (1996).
19. A. Kose and S. Hachisu, *J. Colloid Interface Sci.* **55**, 487-498 (1976).
20. A. P. Gast, W. B. Russel and C. K. Hall, *J. Colloid Interface Sci.* **109**, 161-171 (1986).